Role of Increased Crystallinity in Deformation-Induced Structure of Segmented Thermoplastic Polyurethane Elastomers with PEO and PEO−PPO−PEO Soft Segments and HDI Hard Segments

Ryan S. Waletzko,[†,§,#] LaShanda T. James Korley,[†,§,||,#] Brian D. Pate,[‡,§,⊥] Edwin L. Thomas,[‡,§] and Paula T. Hammond*[,†,§]

Department of Chemical Engineering, Department of Materials Science and Engineering, and Institute for Soldier Nanotechnologies, Massachusetts Institute of Technology, Cambridge, Massachusetts 02139

Received September 30, 2008; Revised Manuscript Received November 26, 2008

ABSTRACT: The phase-segregated nature of polyurethanes allows meaningful connections to be made between morphological and physical properties. We have taken advantage of this behavior by synthesizing a series of polyurethanes with varying extents of crystallinity and studying their morphologies in both the unstrained and deformed states, going from a completely amorphous soft segment to one with similar chemistry that displays a high extent of soft domain crystallization, thus enhancing phase segregation. The presence of dispersed semicrystalline regions within the continuous soft domain has been shown to provide a reinforcing effect when compared to that of a non-crystalline soft segment polyurethane. Incorporating a semicrystalline soft segment (PEO, 1000 g/mol) has been shown to improve overall sample toughness; however, if higher molecular weight PEO soft segments are employed (4600 g/mol), extensibility and, consequently, toughness are adversely affected due to an increased continuous domain modulus. In-situ deformation experiments demonstrate two very different deformation responses. In the copolymer-containing polyurethane (PEO−PPO−PEO, 1900 g/mol), the hard domains retain a tilted configuration up to strains of ∼450%, with only a small fraction of the hard segments undergoing reshuffling. The PEO1000-containing polyurethane, on the other hand, begins to demonstrate meridional scattering at strains of 200%, with it being the dominant peak by a strain of 300%. These two deformation behaviors are indicative of the two primary responses to deformation, which are shear and tensile, respectively. Frequently, a tensile mechanism points to decreased polyurethane mechanical properties, though this phenomenon is not seen in the series of interest.

Introduction

The unique material properties of segmented polyurethanes are directly related to their hierarchical morphology. The response of this microstructure to deformation facilitates an understanding of its toughening mechanism. The deformation behavior of segmented polyurethanes has been studied extensively using a variety of experimental techniques.[1−14] In early investigations, Bonart probed the response of physically cross-linked polyurethane networks to deformation using small-angle and wide-angle X-ray scattering (SAXS and WAXS).[2,3] On the basis of these studies, the tensile alignment of initially randomly oriented soft segment chains exerted a local torque force that orients the hard domains perpendicular to the direction up to 300% strain. Above 300% strain, the nature of the hard segment (crystalline or paracrystalline) strongly influenced the deformation behavior. For paracrystalline MDI−ethylene diamine or MDI−hydrazine hard segments, further elongation resulted in the reorientation and restructuring of the hard domains along the stretch direction as stress is transferred from strain-induced crystalline (PTMO) or paracrystalline (mixed polyesters) soft segments. In crystalline MDI−BDO hard domains (∼40 wt % diisocyanate), the hard segments within hard domains were found to orient along the equator up to 400% strain, which suggested that crystalline hard segments behave as inert fillers during deformation. Bonart also proposed that the hard segment reflections observed in diffraction patterns were due to the sterically hindered lateral arrangement of hydrogen bonds between hard segments due to a pseudocrystalline lattice formation.

Kimura et al. probed further the deformation mechanisms in polyurethaneureas with crystalline hard domains.[7] At low tensile strains, the long axis, which is taken as the length of the lamellae, contributed to scattering at a tilt angle to the direction of elongation. As a result, hydrogen bonding between hard segments also produced alignment at a preferred angle to the deformation. At higher strains, the principal axis was along the length of the hard segment due to the disruption of the crystalline texture, forming nanofibrils and resulting in diffuse scattering along the equator.

Additional SAXS studies of the deformation behavior of the microphase-segregated structure of segmented polyurethanes revealed two dominant response modes of the physically cross-linked network to tensile strain.[1,5] Segmented polyurethanes containing MDI hard segments chain-extended with BDO (37 wt % MDI) and toluene diisocyanate (TDI) hard segments chain-extended with either trimethylene glycol bis(*p*-aminobenzoate) (32 wt % TDI) or 1,1,1-trimethylolpropane (47 wt % TDI) were investigated by Desper and collaborators. From this study, a generalized model based on shape and structural rigidity (hydrogen-bonding, crystallinity) of the hard domain response to deformation was presented.[5] Hard segments with high degrees of structural integrity and cylindrical geometry (length (*L*)/diameter (*D*) ≫ 1) are subjected to a shearing mechanism due to the local torque applied by the aligning of soft segment chains, adopting a preferred tilt angle of the hard domains to applied stress and producing a four-point scattering pattern. In the case of hard domains with *L*/*D* ∼ 1 (cubic) and less ordered

* Corresponding author. E-mail: hammond@mit.edu.
† Department of Chemical Engineering.
‡ Department of Materials Science and Engineering.
§ Institute for Soldier Nanotechnologies, Massachusetts Institute of Technology, Cambridge, MA 02139.
|| Current address: Macromolecular Science and Engineering Department, Case Western Reserve University, Cleveland, OH, 44106.
⊥ Current address: Core Research and Development, The Dow Chemical Company, 1897 Building, Midland, MI 48667.
# These two authors contributed equally to this work.

10.1021/ma8022052 CCC: $40.75
Published on Web 02/24/2009

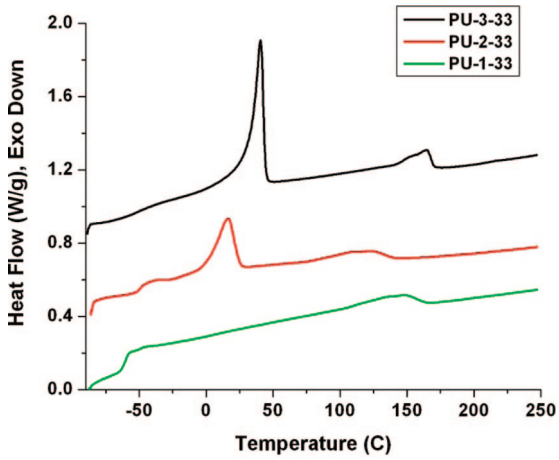

Figure 1. Differential scanning calorimetry data for the polyurethane series. All scans shown are the second heating scan at a heating rate of 10 °C/min.

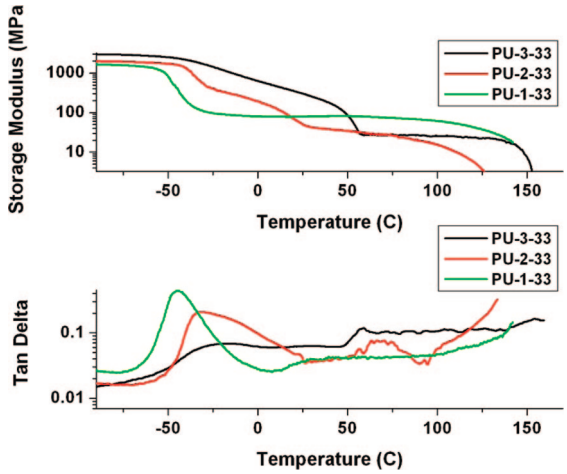

Figure 2. Dynamic mechanical analysis data of polyurethane series are shown. The top figure displays the storage modulus of the samples, while the lower figure provides the loss modulus data via the loss tangent (tan delta). Noise seen in the tan delta data are the likely result of sample thinning during the heating process, leading to an increased signal-to-noise ratio in loss modulus curves.

morphologies, the length of the hard block oriented perpendicular to the elongation, resulting in a two-point scattering pattern along the meridian. Blundell et al. conducted stress−strain studies of thermoplastic polyurethanes containing 42 wt % hard segment.[1] In the polyurethanes containing a lower percentage of aggregated hard segments (less structural rigidity), affine deformation occurred in the polyurethane network, which produced an elliptical pattern with scattering intensity on the meridian and similar to the findings of Desper and co-workers.[5] For the interconnected (structurally rigid) hard domain morphologies, a slightly elliptical four-point pattern was observed due to structural reorganization, which is reminiscent of the shearing mechanism introduced by Desper and co-workers.[5] Elliptical scattering patterns have also been observed and fit by Grubb et al. in other semicrystalline polymer systems during deformation.[15,16]

Segmented polyurethane structural development studies within the past 10 years using in situ synchrotron simultaneous WAXS/SAXS, FT-IR dichroism, and AFM have complemented these initial investigations, adding depth to the knowledge base of polyurethane deformation behavior.[4,9,10,13,17−19] An excellent study of the deformation behavior of segmented polyurethaneureas was conducted by Yeh and co-workers.[13] Yeh et al. concluded that disrupted hard domain lamellae and strain-induced aligned soft segments contribute to equatorial scattering in the low hard segment (12 wt %) polyurethane studied in their research, but the intensity may be decreased due to the lack of electron density contrast between the hard segment fibrils and the aligned soft segment chains and/or the decrease in coherent scattering due to the small size of the broken down lamellae.[13] A recent study by Vaia et al. has shown that soft segments are also capable of demonstrating hard segment-like behavior at low hard segment contents (∼10 wt %).[17] Researchers also probed the contribution of various orientations (perpendicular, parallel, and at angle) of hard domain lamellae orientation on the initial mode of deformation for segmented polyurethanes containing 20−50 wt % HS.[9] Lamellae initially oriented perpendicular to the stretch direction produced an increase in the interdomain spacing under deformation, while those lamellae aligned parallel to the elongation undergo shearing under strain, which causes a decrease in the interdomain spacing. At higher hard segment contents, hard domain destruction occurred at lower strains. In addition, Lee et al. investigated the soft segment conformation using SAXS, concluding that the soft chains are only partially extended at high strains due to the hard domain lamellae breakup.[9]

Table 1. Breakdown of PEO-Containing Polymer Series[a]

polyurethane	soft segment	hard segment
PU-1-33	PEO−PPO−PEO (1900 g/mol)	33 wt %
PU-2-33	PEO (1000 g/mol)	33 wt %
PU-3-33	PEO (4600 g/mol)	33 wt %

[a] From left to right, columns contain polymer name, soft segment identity, and hard segment content, respectively. All polyurethanes consist of hexamethylene diisocyanate−butanediol (HDI−BDO) hard segments.

In a previous work, we detailed the morphological and mechanical behavior of semicrystalline segmented polyurethanes containing varying degrees of order within the continuous domain, proposing that the incorporation of soft segment crystallites contributes to the overall reinforcement of the polyurethane matrix by absorbing energy through a reformable process during deformation.[20] Sonnenschein et al. have demonstrated improved mechanical properties by incorporating semicrystalline polyester diols that possess both a high melting temperature and enthalpy of melting.[21] In this current study, we seek to extend this assessment by resolving the development of the soft segment phase in the deformation-induced microstructure by comparing three segmented polyurethanes with either amorphous or semicrystalline soft segments, but identical hard segment contents. Here, our goal is to observe in-situ and understand how the restructuring of the soft segment phase during deformation affects mechanical behavior as well as to probe the role of ordering within the continuous phase as a toughening mechanism. With this framework, new materials may be designed which achieve high levels of energy absorption through strategic incorporation of soft segment ordering.

Experimental Section

Materials. Segmented polyurethanes containing either poly(ethylene oxide) (PEO; 1000 and 4600 g/mol) or poly(ethylene oxide)−poly(propylene oxide)−poly(ethylene oxide) (PEO−PPO−PEO; 1900 g/mol Pluronic) soft segments and 1,6-hexamethylene diisocyanate−1,4-butanediol (HDI−BDO) hard domains (33 wt %) were used in this investigation. Their synthesis has been described previously.[20] The labeling protocol is as follows: PU-1-33 (PEO−PPO−PEO; 1900 g/mol soft segments), PU-2-33 (PEO; 1000 g/mol soft segments), and PU-3-33 (PEO 4600 g/mol soft segments).

Differential Scanning Calorimetry (DSC). The thermal phase behavior of these thermoplastic polyurethanes was investigated using a TA Instruments Q1000 differential scanning calorimeter,

Table 2. Tabulated DSC Data Show Relevant Thermal Properties for Second Heating Scan

	PU-1-33 (PEO−PPO−PEO)	PU-2-33 (PEO1000)	PU-3-33 (PEO4600)
$T_{g,SS}$ (°C)	−56.6	−50.4	−48.6
$T_{m,SS}$ (°C)		19.3	45.8
$\Delta H_{m,SS}$ (J/g)		28.5	60.6
$T_{m,HS}$ (°C)	147.5	122.5	157.4
$\Delta H_{m,HS}$ (J/g)	7.62	9.5	12.5

operating at a heating and cooling rate of 10 °C/min under a nitrogen atmosphere. As precipitated, unannealed polymer samples were subjected to two heating and cooling cycles between 90 and 250 °C. The second heating cycle yielded metastable morphologies within the polyurethane materials. Transitions were investigated for the second heating and cooling cycles using a linear extrapolation method (T_m) and the midpoint inflection method (T_g). DSC traces of the vacuum-annealed, cast films gave similar transitional data to the precipitated polyurethane materials.

Atomic Force Microscopy (AFM). AFM specimen nanostructure was investigated by a Nanoscope D3100 AFM with a Nanoscope IIIa controller and a multimode scanning probe microscope. Tapping mode phase images of sample surfaces were made using Veeco NanoProbe tips (130 mm, 280−361 kHz). Thin polymer films were spin-cast from dilute solution (1 wt %) and annealed at 60 °C prior to imaging.

Stress−Strain Experiments. The tensile properties of these segmented polyurethanes were determined using a Zwick/Roell Z010 with a 500 N load cell and convex jaw grips with aluminum and flat polyurethane faces to minimize tearing at the grips and film slippage during deformation. Polyurethane films were solvent-cast from 0.05 g/mL (5 wt %) solutions in *N,N*-dimethylacetamide (DMAc) into Teflon molds and allowed to dry for ∼3 days at 60 °C while under a constant N_2 purge of 2 standard cubic feet per hour (scfh). After 3 days, the films were annealed by vacuum drying at 60 °C for ∼1 h prior to use and cooled to room temperature in air. The samples were elongated to failure at 100% of the initial gauge length per minute. Tensile properties were the average of at least three specimens.

Dynamic Mechanical Analysis (DMA). DMA specimens were prepared as described in the tensile testing section above. Thin polyurethane films (∼0.1 mm) were evaluated using a TA Instruments Q800 series DMA over a temperature range of −100 to 250 °C at a frequency of 1 Hz, a ramp rate of 3 °C min^{-1}, an initial strain of ∼0.2%, and amplitude of 10 μm.

Small-Angle and Wide-Angle X-ray Scattering (SAXS and WAXS). SAXS and WAXS data were acquired at the X27C beamline at the National Synchrotron Light Source (NSLS) at Brookhaven National Laboratory or at the G1 beamline at the Cornell High-Energy Synchrotron Source (CHESS). The X27C X-ray wavelength, λ, was 1.366 Å, which was monochromatized from the bending magnet using a double-multilayer (silicon/tungsten) monochromator. The typical flux was 9×10^{11} photons/s. The beam was collimated to a maximum spatial resolution of 100 nm using three pinholes. The relative X-ray intensity was measured before (I_0) and after (I_1) the sample by using proportional counters. The X-ray scattering was detected using a Fuji BAS 2500 imaging plate system, and SAXS and WAXS data were simultaneously measured. At the CHESS G1 beamline, $\lambda = 1.23$ Å, the beam was collimated to a horizontal divergence of 1 mrad via the wiggler "*K*" factor and horizontal-focusing optics. This natural collimation was supplemented by use of two 1 mm slits and a third, which functioned as a guard slit. A MedOptics CCD detector was used to measure the scattered radiation, with pixel size 47.19 μm/pixel and size 1024 × 1024 pixels.

A home-built stretcher was used to elongate continuously the ∼0.1 mm thick samples at 25% of their initial length per minute. Scattering patterns were collected for one second in SAXS and 20 s in WAXS (time-averaged). A dark (blocked beam) pattern was measured for each collection time employed. The appropriate dark pattern was subtracted from each sample and background scattering pattern. Data were reduced from a 2D (intensity vs 2θ, χ) to 1D (intensity vs 2θ) format by integrating over all values of Ψ, for each value of 2θ, where 2θ is the scattering angle and Ψ is the azimuthal angle. SAXS data have been expressed in terms of q, where $q = 4\pi \sin(\theta)/\lambda$. The reduced data were normalized by I_1. Polymer interdomain spacings were obtained by the relationship $q = 2\pi/d$ at selected peak positions of q.

Results and Discussion

Thermal Characterization. Segmented polyurethanes typically display several thermal transitions. The soft domains possess a low-temperature glass transition (often below room temperature) and a melting transition if semicrystalline; the hard segment may also have a glass transition and/or multiple melting transitions due to the distribution of hard segment lengths. The soft and hard domain thermal transitions were investigated via DSC. Second heating scan data were employed to compare morphologies of the as-precipitated polymers. The cast films used for DMA and mechanical property testing demonstrated similar thermal behavior.

DSC thermal analysis of PU-1-33 shows strong microphase segregation, evidenced by a strong glass transition at −57 °C (Figure 1). PU-1-33 possesses a small hard segment melting endotherm centered at ∼147 °C, though the transition is extremely broad and spans a temperature range of 125−150 °C. The presence of the PEO−PPO−PEO copolymer soft segment facilitates strong phase segregation, which was previously shown by Korley et al. via insensitivity to hard segment content (and an increased hard domain melting transition temperature compared with the PEO1000 polyurethane).[20] Also, soft segment crystallinity is suppressed as a consequence of the PPO midblock present in Pluronic copolymers. Soft segments are unable to participate in extensive hydrogen bonding with hard domain sites due to the disruption of regular chain structure, enhancing phase segregation. PPO hydrophobicity and incompatibility with the polar hard block promote hard domain formation.

DSC results of PU-2-33 show a glass transition near −50 °C, though the transition does not display the normal inflection seen for T_g in the other thermoplastic materials, but rather displays a small endothermal peak at the glass transition. PU-2-41, a polyurethane from our previous study which also contains 1000 g/mol PEO soft segments, has shown this same low-temperature transition.[20] The soft segment melting transition occurs at 19 °C, with an enthalpy of melting of 28.5 J/g. Small crystallites are present, as evidenced by the significant discrepancy from the highly crystalline homopolymer PEO melting transition temperature of 65 °C.[22] Enhanced cross-domain hydrogen bonding, and hence increased phase mixing, is frequently seen in polyether polyurethanes due to the presence of interaction sites within both hard and soft polymer regions.[23,24] Well-ordered hard domain crystallites are suppressed, manifest by a lower melting transition temperature. There is a broad hard segment melting transition centered near 120 °C, having peaks at ∼110 and 123 °C and an enthalpy of melting of 9.5 J/g.

The DSC thermogram of PU-3-33 shows a small soft segment glass transition at −48 °C, followed by a strong soft segment melting transition at ∼46 °C and a melting enthalpy of 60.6 J/g, indicative of the highly crystalline nature of its high molecular weight PEO soft segments. The hard segment shows a melting transition with peaks at 157 and 165 °C and a melting enthalpy of 12.5 J/g, which occur at noticeably higher temperatures and have a higher degree of hard domain order than the other polymers in the series. With these high temperature transitions present, the microphase segregation is more extensive than in the other two polyurethanes at similar hard segment weight fractions, with its

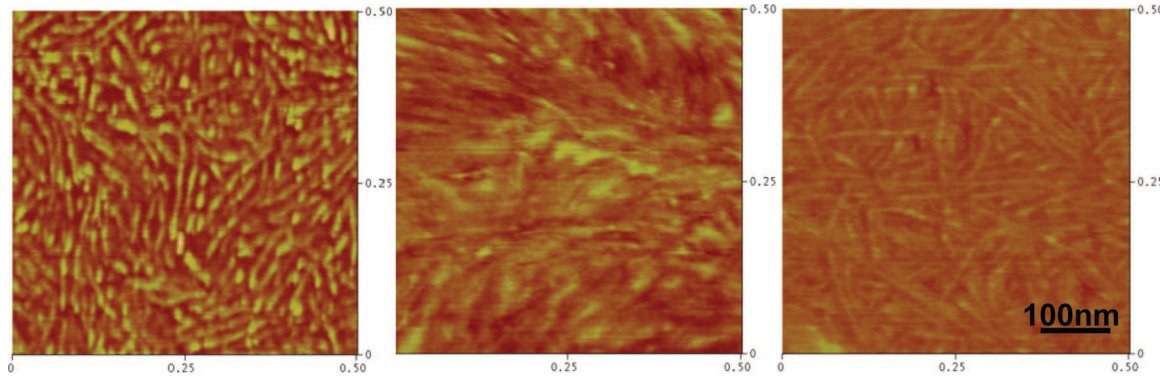

Figure 3. AFM tapping mode phase images of PU-1-33, PU-2-33, and PU-3-33 films from left to right, respectively (annealed 60 °C, 1 h). All scans shown are 500 nm by 500 nm.

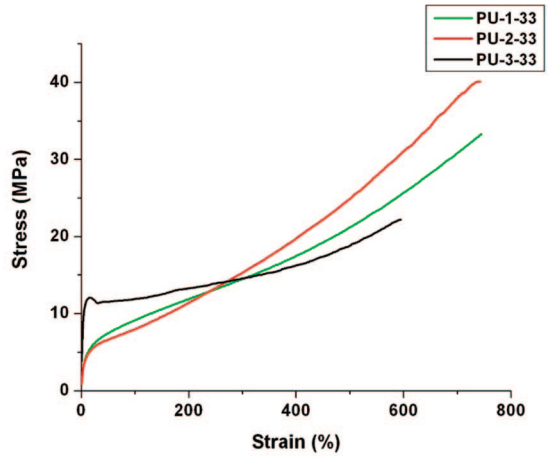

Polyurethane	Elongation at Break (%)	Tensile Strength (MPa)	Young's Modulus (MPa)	Toughness (MJ/m^3)
PU-1-33	700 ± 88	32.1 ± 5.3	69.7	122.1 ± 28.8
PU-2-33	772 ± 54	41.1 ± 3.7	57.4	149.8 ± 31.4
PU-3-33	550 ± 31	21.0 ± 1.1	183.4	83.3 ± 7.1

Figure 4. Mechanical property data of the PU-X-33 series. PU-1-33 and PU-2-33 display very similar mechanical responses, though the PEO1000 polyurethane, PU-2-33, shows a stronger tendency to strain harden at extensions above 200%. PU-3-33, with the highest soft segment molecular weight, displays a tendency to yield at low strains, followed by a necking process until it has propagated through the entire sample. The yielding results from the high extent of soft segment crystallinity present within the sample.

soft segment crystallinity largely responsible for the demonstrated behavior. The enthalpy of crystallization has been shown to be a very strong driving force in block copolymer phase segregation.[25,26] The increase seen in the soft segment melting transition is evidence of enhanced chain crystallization due to increased block incompatibility and soft segment molecular weight, providing a driving force for a better defined interface between hard and soft domains. The less pronounced low-temperature glass transition is a product of having a smaller quantity of amorphous soft segments present within the material. Enhanced hard domain phase segregation leads to a marked increase in hard domain melting temperature and enthalpy of fusion.

Thermomechanical Behavior. Polyurethane dynamic mechanical behavior was used to investigate both thermal transitions and material stiffness. Storage modulus values, signified by E', yield information about material stiffness, while tan delta measures the extent of molecular mobility. In all materials the glass transition temperature was defined as the α transition in the tan delta curve. PU-1-33 shows classic thermoplastic elastomer behavior via a strong glass transition at −50 °C; this α transition appears as an intense peak in tan delta (Figure 2). PU-2-33 has a less pronounced (and broadened) soft segment relaxation. The broad tan delta transition seen in PU-2-33 results from a retardation of molecular mobility by hard domains and soft segment crystallites. Its thermomechanical behavior is similar to that seen for other semicrystalline polymers.[27] PU-3-33 possesses a small glass transition due to its highly crystalline soft domain character. Both PEO homopolymer-containing polyurethanes display broadened tan delta transitions that point toward a retarded molecular mobility that results from interacting crystallites present within both the hard and soft domains.

After its initial glass transition, PU-1-33 has an extremely level rubbery plateau region in its storage modulus until failure at ca. 140 °C. The amorphous block copolymer soft segment is allowed to move freely without matrix flow, a consequence of the well-segregated morphology demonstrated in DSC. The soft

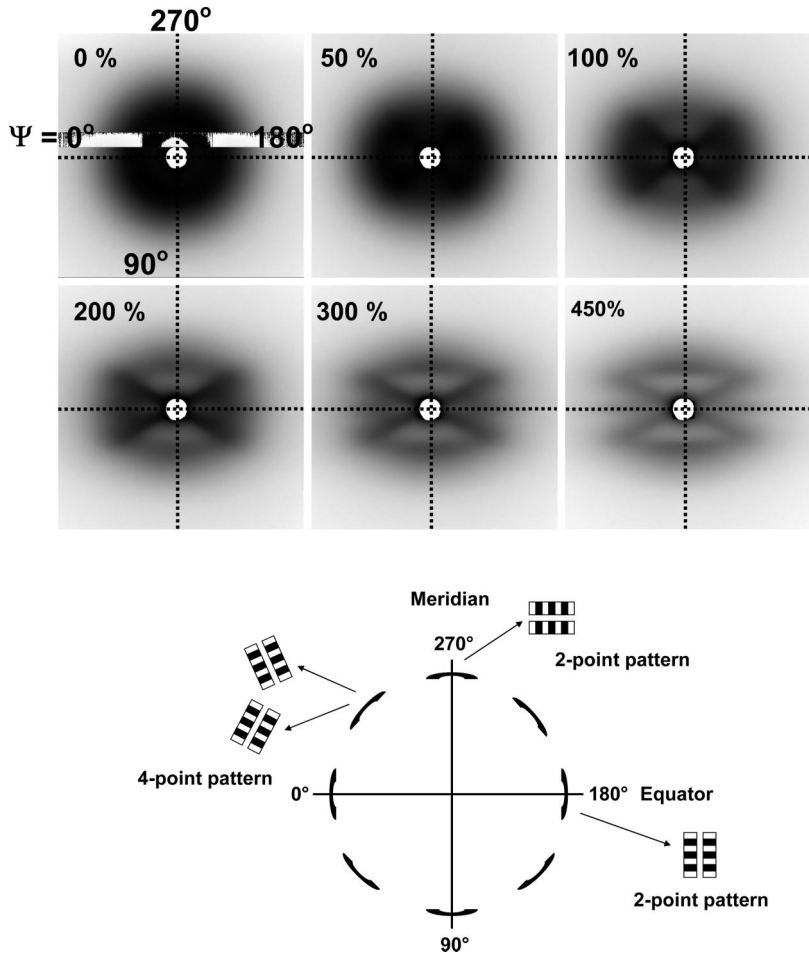

Figure 5. (a) 2D plots of the corrected synchrotron SAXS data of an in-situ deformed film of PU-1-33. The azimuthal angle, Ψ, is defined in the 0% strain plot. (b) Cartoon detailing origin of peaks in small-angle X-ray scattering, adapted from ref 6. The longer rectangles represent hard domains, while the smaller internal rectangles are individual hard segments. Soft segments have been omitted for visual clarity.

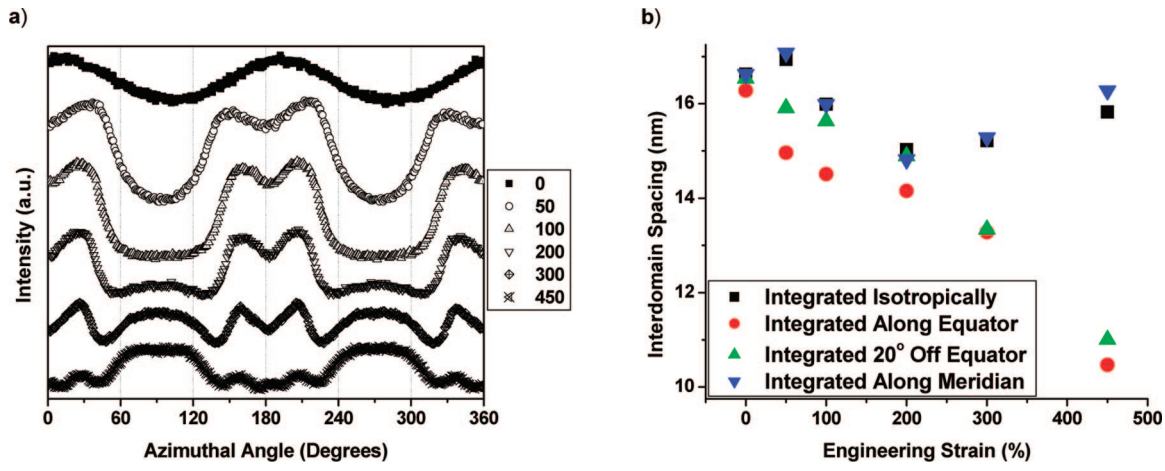

Figure 6. (a) Azimuthal angle (Ψ) profiles of the 2D plots depicted in Figure 5a. For each profile, the mean value of q is 0.42 nm^{-1} and the q range is ±0.05 nm^{-1}. (b) Interdomain spacings of PU-1-33 during deformation, integrated along different paths. For non-isotropic integrations, regions were integrated at ±10° from the center line.

domain melting transition is completely suppressed due to the presence of a PPO midblock in the soft segments. In semicrystalline polyurethane systems, the storage modulus presents a measure of the role of soft segment ordering on their viscoelastic response. The broad glass transition of PU-2-33 is followed by a broad melting peak that ultimately levels off at 25 °C. As the temperature increases past its soft segment melting transition, PU-2-33 displays a decrease in storage modulus until ultimate material failure at 125 °C. Increased phase mixing prevents formation of large hard domain aggregates that serve to anchor amorphous polymer regions at elevated temperatures, though the dispersed soft segment crystallites reinforce the polymer matrix at temperatures below their melting transition; when present, well-defined hard segment regions provide an extended rubbery plateau prior to melting of the high transition temperature region. Crystalline regions of the soft domain serve as reinforcing fillers and impart an enhanced polyurethane mechanical integrity, though cannot prevent material flow at

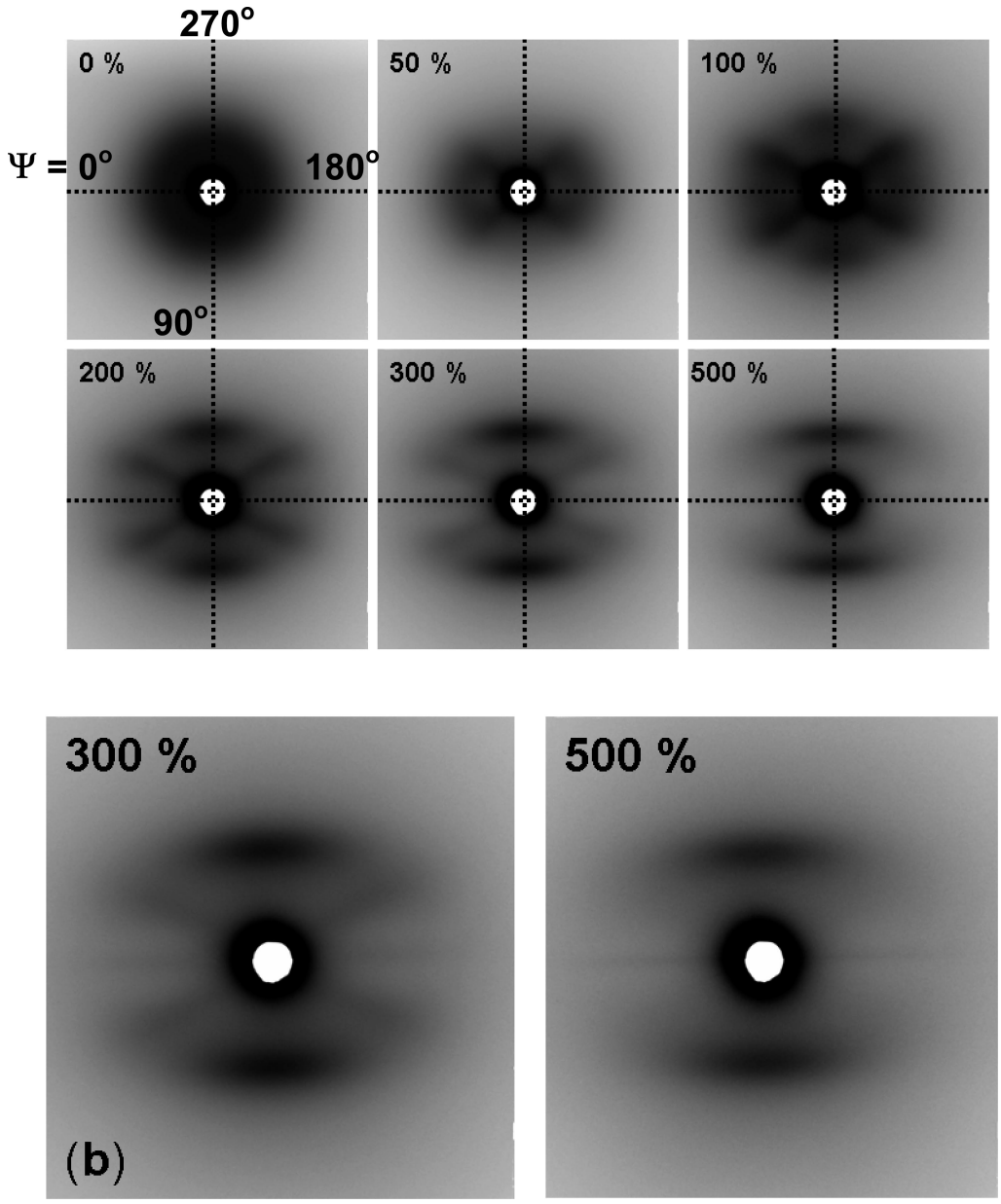

Figure 7. (a) 2D plots of the corrected synchrotron SAXS data of an in-situ deformed film of PU-2-33. The time- and ensemble-averaged strains of each data set are listed. The azimuthal angle, Ψ, is defined in the 0% strain plot. (b) 2D scattering images at 300% and 500% are enlarged without axes to demonstrate the equatorial streaking that coincides with nanofibril formation at high strains.

temperatures significantly above 25 °C. The middle AFM image in Figure 3 shows a lack of well-defined hard segment connectivity, a necessary component for the extended rubbery modulus prior to hard segment melting. Much like PU-2-33, PU-3-33 displays a storage modulus characteristic of semicrystalline polymers, with the majority of its crystalline domains melting at 50 °C. PU-3-33 has an extended rubbery plateau resulting from a strong incompatibility between hard and soft domains, a phenomenon that facilitates aggregation of hard segments to provide further physical cross-linking. The polymer yields at a temperature of 150 °C which is equivalent to the high-temperature DSC melting transition from the previous section.

Atomic Force Microscopy. High modulus regions (hard domains and crystalline soft segments) appear as bright regions in atomic force microscopy while amorphous soft domains are dark, consistent with previous polyurethane systems.[28] The AFM image of PU-1-33 possesses a rod-like structure beneath the bulk surface but has the look of elliptical aggregates bundled together (Figure 3). Rod-like structures seen in the scan are characteristic of the long axis of paracrystalline hard domains.[29] Hard segment boundaries are well-resolved due to PEO block incompatibility with the PPO midblock, preventing large-scale interdomain hydrogen bonding between hard and soft segments. PU-2-33 shows dispersed rod-like segments, but the resolution is much lower, a function of the decreased sample phase segregation compared to other polymers within the series. Increased interphase mixing is demonstrated by movement of the low-temperature glass transition to higher temperatures, as was seen in DSC. Irregular clusters of hard domains and more diffuse domain boundaries originate from polymer phase mixing in the form of hydrogen bonding between hard and soft regions of the polymer, which is commonly seen in polyether polyurethanes.[30] PU-3-33 displays a rod-like structure comparable to that seen at high hard segment content in other HDI−BDO hard segment systems[14,28,31−34] despite its relatively low concentration of hard segments. The crystallinity of the high molecular weight soft segment (4600 g/mol) provides a strong driving force

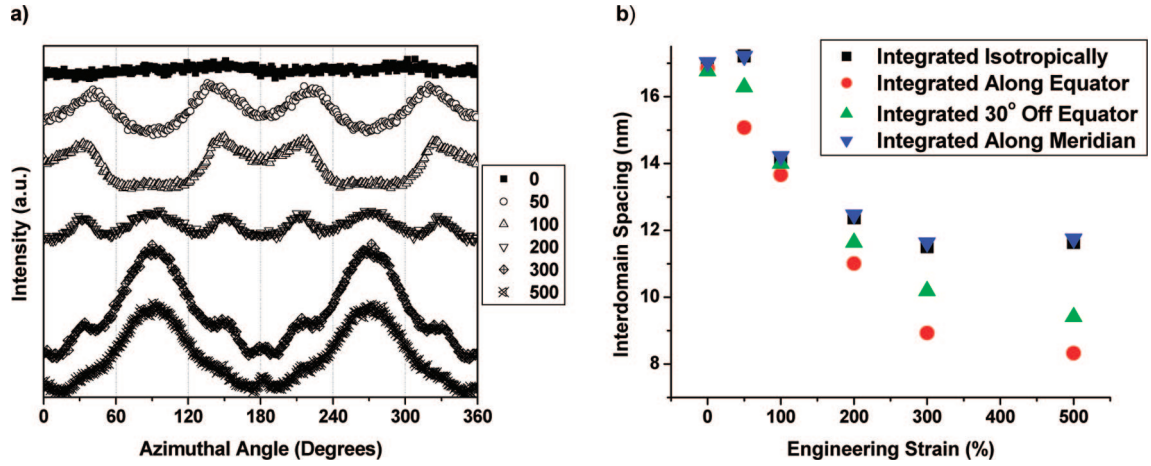

Figure 8. (a) Azimuthal angle (Ψ) profiles of the 2D plots depicted in Figure 7a. For each profile, the mean value of q is 0.47 nm^{-1} and the q range is ± 0.10 nm^{-1}. (b) Interdomain spacings of PU-2-33 during deformation, integrated along different paths. For non-isotropic integrations, regions were integrated at $\pm 10°$ from the center line.

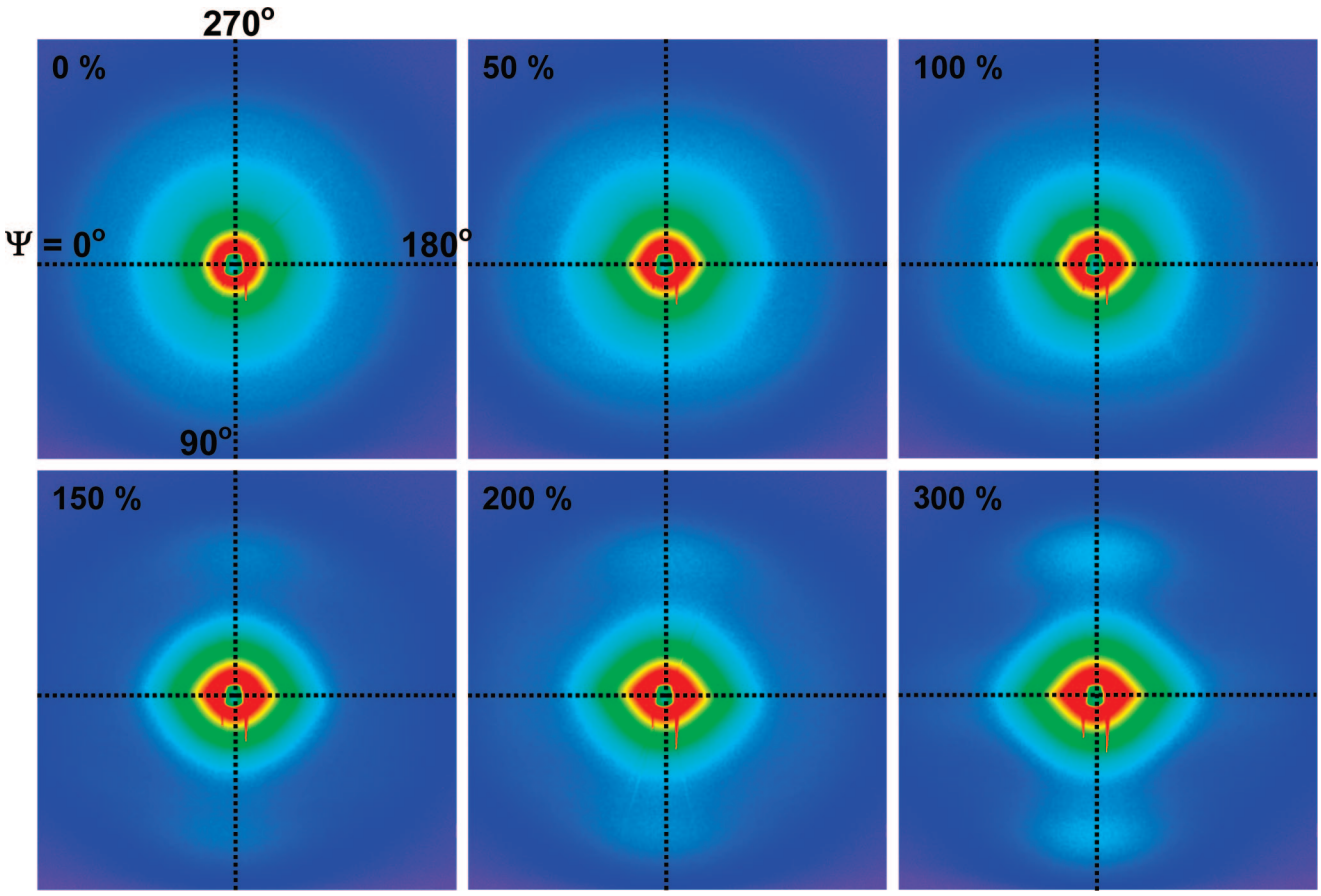

Figure 9. 2D plots of the corrected synchrotron SAXS data of an in-situ deformed film of PU-3-33. The azimuthal angle, Ψ, is defined in the 0% strain plot. A color scale was employed to provide better peak contrast.

for microphase segregation, yielding long, well-defined hard phases within the observed morphology that have dimensions of 10 nm by 100 nm. As a result of its high soft segment crystallinity, PU-3-33 displays a morphology that is attributed to both hard domains and highly ordered soft segment regions. The contrast between the light and dark regions is not as pronounced as many interconnected morphologies due to the small concentration of amorphous soft segment in the continuous polyurethane matrix. Normally, well-defined hard segments appear as the polyurethane transitions from a soft segment continuous to interconnected hard segment morphology.[35]

Mechanical Behavior. Mechanical performance of the PEO-containing polymer series was evaluated by measuring extensibility, toughness, tensile strength, and Young's modulus. In segmented polyurethane systems, hard segments engage in hydrogen bonding to form reinforcing hard domains for the continuous soft segment continuous matrix. PU-1-33 tensile tests yield ultimate strains of 700 ± 88%, along with a tensile strength of 32.1 ± 5.3 MPa (Figure 4). Young's modulus and toughness for these experiments are ~69.7 MPa and ~122.1 ± 28.8 MJ/m^3, respectively. PU-2-33 exhibits typical elastomer behavior (strain hardening), shown via increasing stress during deforma-

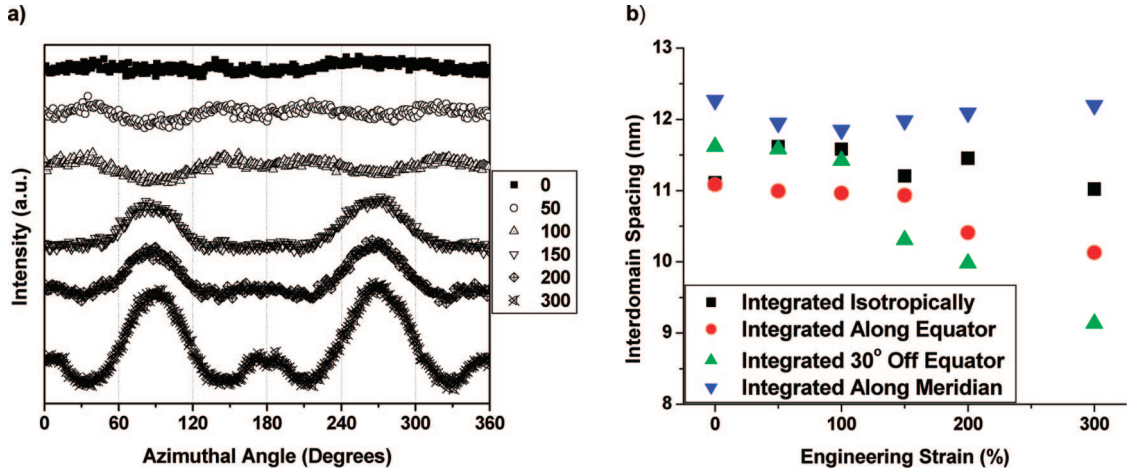

Figure 10. (a) Azimuthal angle (Ψ) profiles of the 2D plots depicted in Figure 9. For each profile, the mean value of q is 0.54 nm^{-1} and the q range is ±0.05 nm^{-1}. (b) Interdomain spacings of PU-3-33 during deformation, integrated along different paths. For non-isotropic integrations, regions were integrated at ±10° from the center line.

tion until sample failure at extensions near 700% of the initial length. The initial yield stress is low, likely resulting from phase mixing present in the morphology, as was previously seen in a similar PEO1000-containing polyurethane system.[20] Tensile deformation experiments revealed an extensibility of 772 ± 54%, with a tensile strength of 41.1 ± 3.7 MPa. The stress−strain curves of PU-2-33 gave a value of 57.4 MPa for the Young's modulus, with a toughness of 149.8 ± 31.4 MJ/m^3. High sample toughness stems from small dispersed PEO crystallites which serve as an additional load-bearing phase. Crystallites are afforded an opportunity to re-form during deformation, a product of the sample possessing a room temperature melting transition. PU-3-33 shows a strong tendency to neck during deformation, yielding higher ultimate strains (550 ± 31%), but without large stress increases aside from the pre-necking portion of the system. Specimens have a waxy feel and opaque appearance, a product of their high PEO crystallinity. The presence of a well-ordered material yields semicrystalline mechanical property behavior during deformation. Tensile experiments gave a Young's modulus of 183.4 MPa and toughness of 83.3 ± 7.1 MJ/m^3. PU-3-33, with the highest soft segment crystallinity, shows the lowest overall extensibility due to the high modulus of the largely crystalline soft segment domains that permeate the structure. These domains, when coupled with the high transition temperature of the minority hard domains, yield a material that deforms plastically at very low deformations (strains greater than 5%). PU-1-33 displays remarkably similar mechanical properties to PU-2-33, which is a likely result of its enhanced phase segregation, allowing aggregation of hard domains to serve as reinforcing fillers.

In-Situ Deformation Studies. *SAXS.* PU-1-33 has an isotropic scattering pattern that becomes increasingly anisotropic with increasing sample strain (Figure 5a). The characteristic hard segment arrangements responsible for scattering peaks are depicted in Figure 5b. At 50% strain, the scattering intensity has shifted toward the equator, indicating that hard segment lamellae are orienting in response to deformation of the amorphous soft segment. Further stretching to 100% produces a four-point pattern (Figure 6a), with the preferred tilt being produced by local torques exerted within the strained soft segments. Near failure strain, the domains are still aligned at a preferred tilt angle from the stretch direction. The four-point scattering pattern results from the previously reported shearing mechanism.[7] As strain is increased to values of 300% and greater, meridional scattering appears, a phenomena that coincides with the beginning of hard domain reorganization. Soft segments that are near failure strain transfer stress to the largely undeformed hard segments, yielding either a shearing or tensile force which is capable of breaking domain hydrogen bonds. PU-1-33 fails prior to complete hard segment reorganization, as evidenced by persistent four-point scattering peaks at high strain. Large-scale hard segment breakup is demonstrated by a two-point pattern on the meridian, where scattering results from periodic ordering of disrupted lamellae in the stretch direction (Figure 5b). During deformation, interdomain spacings in equatorial regions decrease markedly compared to those along the meridian (Figure 6b). PU-1-33 shows a small increase in scattering intensity in the meridional direction with increasing strain. As PU-1-33 is initially stretched, both the isotropically integrated and meridional periodicities remain near a spacing of 16 nm. An initial increase in the long period at 50% strain precedes modest hard domain restructuring at 100%. Small extents of hard domain reorganization continue up to strains of 200%, followed by increases in the long period until 450%. Domain spacing increases seen at high strain are attributed to a correlation between newly formed hard domains that undergo a spacing increase as the polymer is deformed. Equatorial scattering spacing decreases steadily with strain in the polyurethane, as hard domain lamellae that are initially oriented in the direction of strain undergo a shearing process that continuously shrinks the interdomain spacing. These lamellae show a decrease in interdomain spacing from 16.5 nm in the undeformed state to ~11 nm at 450% strain. Similar conclusions can be made for hard domains that are oriented in intermediate directions that are slightly off-parallel. Lamellae will initially align in the direction of stretch, followed by a shear deformation of the area between these domains prior to full-scale hard segment reorganization.

PU-2-33 and its initially isotropic scattering pattern quickly display anisotropy in the form of four-point scattering at strains of 50%. By a strain of 200%, meridional scattering begins to appear and coincides with the beginning of hard segment reorganization. As strain is increased to 300%, the initial four-point scattering indicative of tilted lamellae has almost completely disappeared, meaning that the majority of the hard domains have undergone reorganization (Figure 7a). Also of note is the equatorial streaking that appears at these strains, characteristic of the beginning of oriented nanofibril formation (Figures 7b and 8a). The enlarged scans at 300% and 500% strain (Figure 7b) in particular display this phenomenon. Azimuthal plots shown in Figure 8a at these strains also show small peaks at the equator which correspond to the nanofibril streaks. PU-2-33 displays a small initial increase in domain spacing, followed by a pronounced decrease along all integration

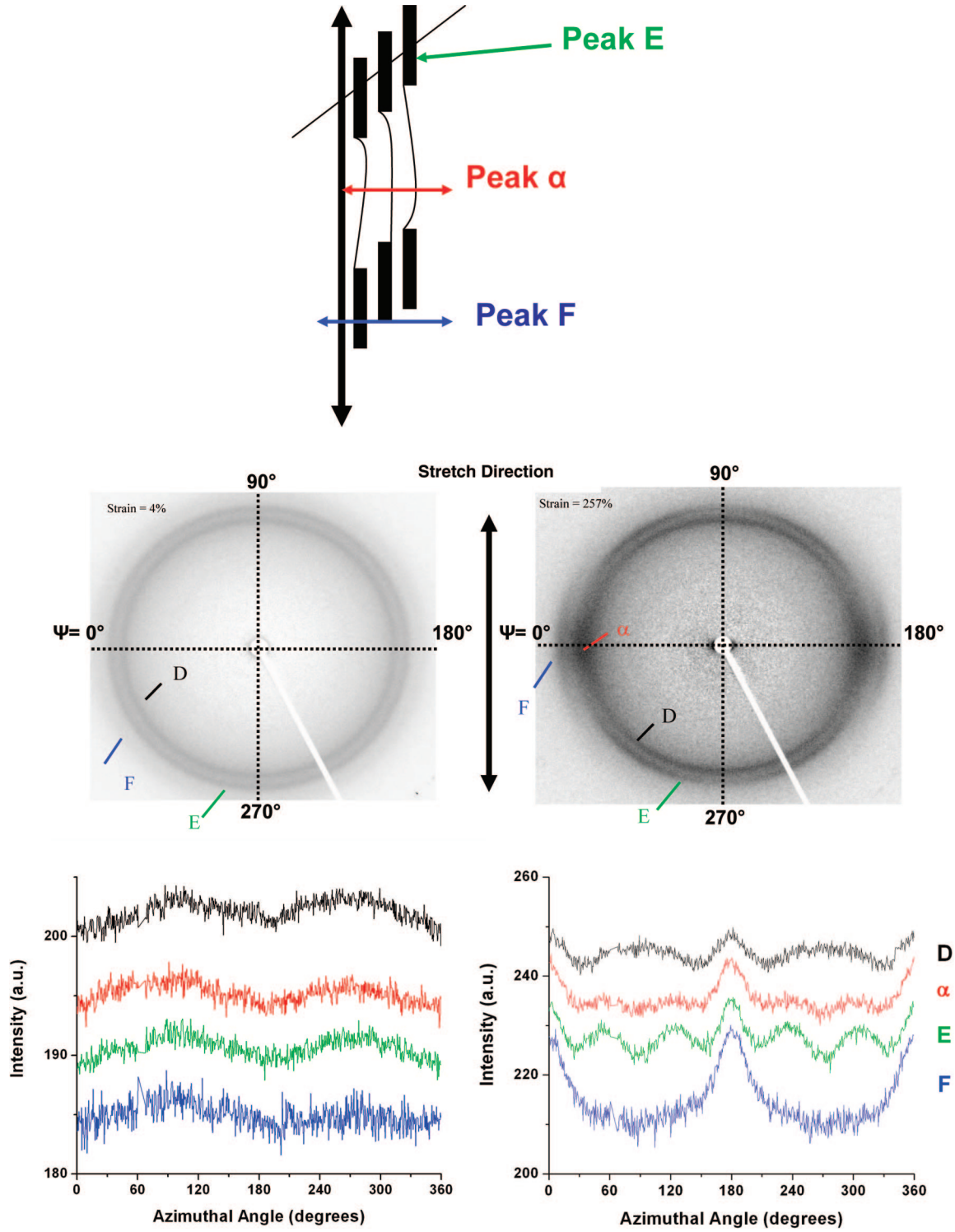

Figure 11. (a) Origin of peak reflections in wide-angle X-ray scattering (WAXS) in PEO polyurethane series. (b) 2D plots of the corrected synchrotron WAXS data of an in-situ deformed film of PU-1-33. As the sample is deformed, four prominent reflections appear at spacings of D ($2\theta = 19.6°$, 4.4 Å), E ($2\theta = 21.3°$, 4.1 Å), and F ($2\theta = 23.6°$, 3.8 Å) and α ($2\theta = 20.6°$, 4.2 Å).

directions (Figure 8b). The most prominent difference between PU-2-33 and PU-1-33 is seen in the steep initial domain spacing decreases during deformation from the unstrained state. Diminishing interdomain correlation lengths are demonstrated by downward slopes of both the isotropic and meridional line scans in Figure 8b. Interdomain spacings in the two regions steadily decrease from 17 nm initially to 12 nm at 300% strain, at which point a plateau is reached. Equatorial and off-equatorial integrations tend toward spacings of 8.3 and 9.4 nm, respectively, evidence of the large amount of shearing deformation that occurs between domains oriented parallel to the stretch direction. Downward trends in PU-2-33 interdomain spacing do not necessarily translate to deteriorated mechanical properties, which is contrary to what is normally seen in polyurethanes.

The initially isotropic scattering pattern of PU-3-33 develops a weak four-point scattering pattern at low strains, up to 100% strain (Figure 9). Rigid polymer regions display plastic deformation by a strain of 150%, evidenced by strong two-point scattering on the meridian (Figure 10a). The strong meridional scattering, coupled with the disappearance of the initial four-

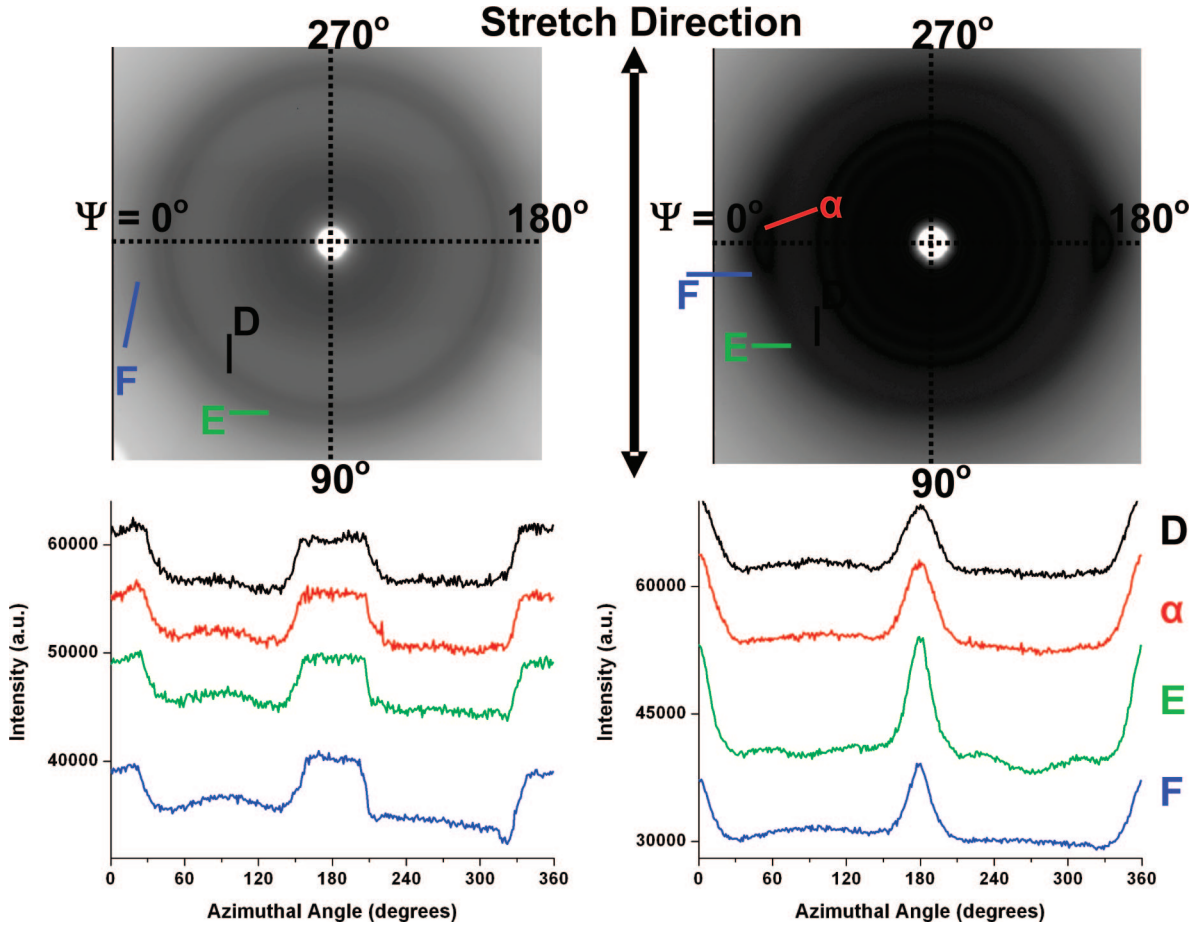

Figure 12. 2D plots of the corrected synchrotron WAXS data of an in-situ deformed film of PU-2-33. As the specimen is deformed, three peaks are discernible, though the resolution is limited by the breadth of the primary alpha reflection. The labeled peaks are D ($2\theta = 16.1°$, 4.4 Å), E ($2\theta = 17.3°$, 4.1 Å), and F ($2\theta = 20.9°$, 3.4 Å) As the specimen is strained, a broad, prominent peak, α($2\theta = 16.9°$, 4.2 Å), appears, which tends to obscure the resolution of the initial peaks.

point scattering, indicates large scale disruption of the initially ordered cross-linking regions, which are primarily attributed to soft segment crystallites at room temperature. Ordered crystalline regions in semicrystalline polyethylene[36] and segmented polyurethanes[17] have demonstrated similar responses to deformation to those of paracrystalline hard segments when probed by SAXS. As has been recently shown by Vaia et al.,[17] the soft segment crystallinity is the major contributor during unixial deformation, with the hard segments acting concurrently to further reinforce the polymer matrix. Semicrystalline polymer systems that are isotropically oriented have displayed scattering patterns that combine the responses of domains that are aligned both parallel and transverse to the strain direction.[36] As PU-3-33 is deformed, soft segments do not possess adequate mobility to efficiently transfer stress from the continuous matrix to its hard domains without disrupting their long-range order. Supporting Information Figure S1 provides further evidence of the long-range order of PU-3-33, showing multiple scattering peaks in a 1D SAXS plot. PU-3-33 displays little change in domain spacing in both the isotropic and meridional directions during deformation, with values ranging from 11.5 to 12 nm throughout the stretching process, which can be seen in Figure 10b. This trend is expected due to its nonelastomeric behavior during strain, with a neck that propagates throughout the film prior to ultimate failure. Equatorial and off-equatorial regions show a decreased domain spacing while stretched (11 and 11.5 nm to 10 and 9 nm, respectively), further supporting the notion that scattered regions shrink as a result of shearing processes during deformation.

WAXS. A generalized cartoon provides periodicities for the origin of reflections seen in polyurethane PU-1-33 (Figure 11a), in which only three wide-angle scattering peaks are observed initially (Figure 11b). Peaks labeled D ($2\theta = 19.6°$, 4.4 Å), E ($2\theta = 21.3°$, 4.1 Å), and F ($2\theta = 23.6°$, 3.8 Å) correspond to hard segment crystalline or paracrystalline spacings. As the polymer film is elongated, an additional ordering contribution on the equator becomes apparent at $2\theta = 20.6°$ (4.2 Å). This spacing is a result of alignment of the PEO−PPO−PEO soft segment chains and becomes more prominent with increased strain. Interpretation of the development of hard domain crystallization is complicated by the small separation of peaks D, E, and α and the breadth of the α peak. The α peak contributes to the azimuthal plots of each peak due to its broadness. Peak D (4.4 Å) aligns parallel to the stretch direction and corresponds to a crystalline spacing along the HDI−BDO chain axis. Peak E (4.1 Å) initially aligns along the equator, though at higher strains adopts a four-point scattering pattern at ±30°, likely due to the spacings between the long axis of the spherulitic hydrogen-bonded hard domain aggregates. The equatorial scattering peak F (3.8 Å), which becomes more prominent with increased strain, is due to spacing between extended fibrils of HDI−BDO chains. The persistence of the initial scattering peaks at 250% strain suggests that disruption of the crystalline, hydrogen-bonded domains has not occurred.

In PU-2-33, three peaks are present in the wide-angle X-ray scattering pattern, D ($2\theta = 16.1°$), E ($2\theta = 17.3°$), and F ($2\theta = 20.9°$), which correspond to hard segment crystalline or paracrystalline spacings of 4.4, 4.1, and 3.4 Å, respectively (Figure 12). As the specimen is strained, a broad, prominent peak, α, appears, centered at $2\theta = 16.9°$ ($d = 4.2$ Å), which overlaps the spacing range for all three initial peaks, complicat-

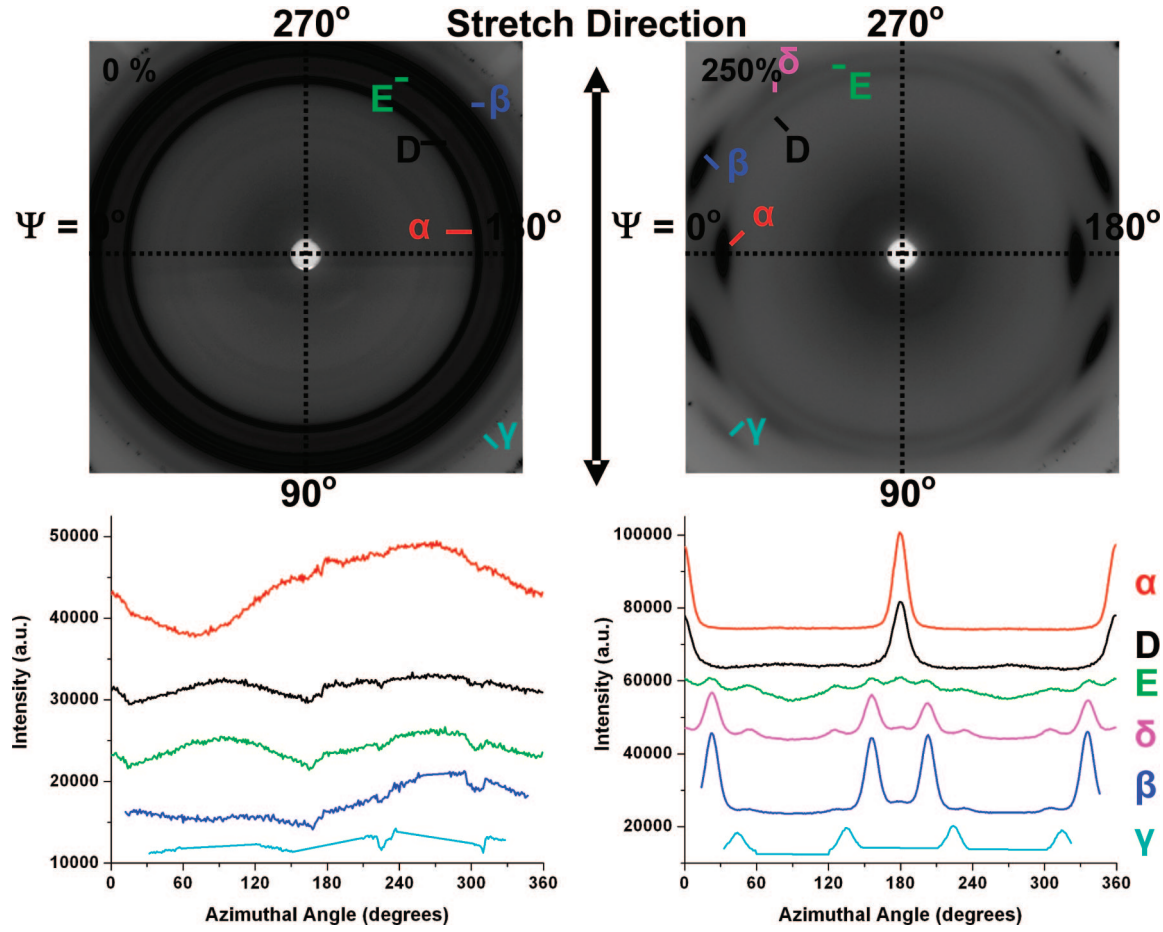

Figure 13. 2D plots of the corrected synchrotron WAXS data of an in-situ deformed film of PU-3-33. As the specimen is deformed, five peaks are seen. D (2θ = 16.4°, 4.3 Å) and E (2θ = 17.8°, 3.9 Å), where peaks D and E are crystalline or paracrystalline hard domain spacings of the HDI−BDO; α (2θ = 15.3°, 4.63 Å), β (2θ = 18.6°, 3.81 Å), and γ (2θ = 21.0°, 3.38 Å) correspond to crystalline PEO reflections, with δ (2θ = 18.0°, 3.94 Å) being another PEO crystal peak that becomes more pronounced with strain.

ing resolution of the initial peaks during deformation. The high degree of phase mixing present in the sample yields a much lower signal-to-noise ratio than seen for the other polyurethanes, which is a likely cause of the limited resolution present in azimuthal scans. Peaks have a tendency to migrate toward the equator upon sample deformation. This result is most likely due to a deficiency of well-defined hard domain aggregates, a consequence of the high degree of hydrogen bonding between hard segment and soft segment chains.

In PU-3-33, five peaks are initially visible in the undeformed sample, as shown in Figure 13: D (2θ = 16.4°, 4.3 Å) and E (2θ = 17.8°, 3.9 Å), where peaks D and E are crystalline or paracrystalline hard domain spacings of the HDI-BDO; α (2θ = 15.3°, 4.63 Å), β (2θ = 18.6°, 3.81 Å), and γ (2θ = 21.0°, 3.38 Å) correspond respectively to the (120), (032), and (024) reflections along the fiber axis of a PEO crystallite.[37] A morphology dominated by soft segment crystallinity is expected for the PU-3-33 system given its large volume fraction and highly crystalline character. As the specimen is strained, a weak reflection, δ (2θ = 18.0°, 3.94 Å), appears at an angle of ±35° from the strain direction and is the (004) PEO crystal reflection. Peak D (4.3 Å) aligns transverse to the stretch direction and corresponds to a crystalline spacing along the HDI−BDO chain axis. Peak E (3.9 Å) adopts a weak four-point scattering pattern centered at ±40°, a consequence of periodic spacings between tilted long axes of hydrogen-bonded hard domain. The equatorial scattering peak α (4.57 Å), which becomes more prominent with increased strain, is due to the primary (120) reflection of the PEO crystallite fiber axis. Another intense peak, β, is seen at ±67° from the stretch direction at a spacing of 3.78 Å and comes from the (032) PEO crystal reflection. Similarly, the (024) PEO crystal reflection (γ) becomes visible with strain at an angle of ±45° from the meridian with a spacing of 3.32 Å. Persistence of the initial hard segment scattering peaks at 250% strain suggests that complete disruption of the crystalline, hydrogen-bonded domains has not occurred prior to film failure; however, the close correspondence of the strained specimen to a PEO fiber pattern implies a large degree of soft segment orientation upon uniaxial deformation.[37]

Conclusions

We have investigated the role of soft segment ordering in polyurethane mechanical properties and morphology. In a previous study, we demonstrated that moderate soft segment ordering led to enhanced mechanical properties. By better understanding their response to deformation, we are able to formulate a template for mechanically enhanced polyurethanes. Increasing soft segment molecular weight and crystallinity contribute to an increased incompatibility between the hard and soft domains. In the PEO series, there is a balance between phase segregation and domain ordering that results in the most desirable mechanical properties. PU-2-33, a polyurethane with a low molecular weight PEO homopolymer soft segment and the highest incidence of interdomain hydrogen bonding, possesses the highest toughness of all polymers within the series. The presence of crystallites with a room temperature melting transition allows the formation of reversible matrix reinforcements during deformation due to soft segment chain mobility, allowing these newly formed junctions to serve as load-bearing

phases within the continuous domain. The polyurethane with the largest extent of soft segment crystallinity, PU-3-33, demonstrates a strong tendency to phase segregate under normal processing conditions. By having a melting transition that is well above room temperature (50 °C), the polyurethane network sacrifices extensibility during mechanical deformation. Strong, well-defined reflections in wide-angle X-ray scattering indicate a strongly ordered structure at strains below 300%. Also, with its highly crystalline soft segments, PU-3-33 demonstrates a switch in scattering contrast derived from these ordered domains that is most clearly seen in wide-angle X-ray scattering experiments. PU-1-33, despite not having any soft segment crystallinity, is capable of achieving strains that are comparable with PU-2-33. The highly extensible network is a product of its strong phase segregation due to its copolymer soft segment. Interdomain hydrogen bonding is suppressed by the poly(propylene oxide) soft segment midblock, leading to hard domains that possess a longer persistence length due to more regular hard segment packing. As seen in the structure evolution during deformation, there is a balance of domain ordering which provides optimal mechanical behavior. If the continuous domain has a highly crystalline character, the matrix is unable to properly transfer stress at intermediate strains, lowering the ultimate strains achieved during deformation. By employing a moderate degree of soft domain crystallinity, the polyurethane is allowed to approach higher extents of deformation, enabling use of its ordered structures as a load-bearing phase.

Acknowledgment. This research was supported by the US Army through the Institute for Soldier Nanotechnologies and its facilities under Contract DAAD-19-02-0002 with the US Army Research Office. This work is based upon research conducted at the Cornell High Energy Synchrotron Source (CHESS), a center supported by the National Science Foundation and the National Institutes of Health/National Institute of General Medical Sciences under award DMR-0225180. Research was also carried out at the National Synchrotron Light Source, Brookhaven National Laboratory, which is supported by the US Department of Energy, Division of Materials Sciences and Division of Chemical Sciences, under Contract DE-AC02-98CH10886.

Supporting Information Available: 1D SAXS pattern of PU-3-33 (Figure S1). This material is available free of charge via the Internet at http://pubs.acs.org.

References and Notes

(1) Blundell, D. J.; Eeckhaut, G.; Fuller, W.; Mahendrasingam, A.; Martin, C. Real time SAXS/stress-strain studies of thermoplastic polyurethanes at large strains. *Polymer* **2002**, *43* (19), 5197–5207.
(2) Bonart, R. X-Ray Investigations Concerning the Physical Structure of Cross-Linking in Segmented Urethane Elastomers. *J. Macromol. Sci., Phys. Ed.* **1968**, *B2* (1), 115–138.
(3) Bonart, R. M. L.; Hentze, G. X-Ray Investigations Concerning the Physical Structure of Cross-Linking in Urethane Elastomers. II. Butanediol As Chain Extender. *J. Macromol. Sci., Phys. Ed.* **1969**, *B3* (2), 337–356.
(4) Curgul, S.; Yilgor, I.; Yigor, E.; Erman, B.; Cakmak, M. Effect of chemical composition on large deformation mechanooptical properties of high strength thermoplastic poly(urethane urea)s. *Macromolecules* **2004**, *37* (23), 8676–8685.
(5) Desper, C. R.; Schneider, N. S.; Jasinski, J. P.; Lin, J. S. Deformation of microphase structures in segmented polyurethanes. *Macromolecules* **1985**, *18* (12), 2755–2761.
(6) James-Korley, L. T. Massachusetts Institute of Technology. Dept. of Chemical Engineering. PEO-containing copolymers as polyurethane soft segments in the development of high performance materials. Thesis Ph.D., Massachusetts Institute of Technology Dept. of Chemical Engineering, **2005**.
(7) Kimura, I.; Ishihara, H.; Ono, H.; Yoshihar, N.; Nomura, S.; Kawai, H. Morphology and Deformation Mechanism of Segmented Poly-(Urethaneureas) in Relation to Spherulitic Crystalline Textures. *Macromolecules* **1974**, *7* (3), 355–363.
(8) Laity, P. R.; Taylor, J. E.; Wong, S. S.; Khunkamchoo, P.; Norris, K.; Cable, M.; Andrews, G. T.; Johnson, A. F.; Cameron, R. E. A 2-dimensional small-angle X-ray scattering study of the microphase-separated morphology exhibited by thermoplastic polyurethanes and its response to deformation. *Polymer* **2004**, *45* (15), 5215–5232.
(9) Lee, H. S.; Yoo, S. R.; Seo, S. W. Domain and Segmental Deformation Behavior of Thermoplastic Elastomers Using Synchrotron SAXS and FTIR Methods. *J. Polym. Sci., Part B: Polym. Phys.* **1999**, *37* (22), 3233.
(10) McLean, R. S.; Sauer, B. B. Nano-deformation of Crystalline Domains during Tensile Stretching Studied by Atomic Force Microscopy. *J. Polym. Sci., Part B: Polym. Phys.* **1999**, *37*, 859.
(11) Seymour, R. W.; Allegrez.Ae; Cooper, S. L. Segmental Orientation Studies of Block Polymers 0.1. Hydrogen-Bonded Polyurethanes. *Macromolecules* **1973**, *6* (6), 896–902.
(12) Sung, C. S. P.; Hu, C. B. Orientation Studies of Segmented Polyether Poly(Urethaneurea) Elastomers by Infrared Dichroism. *Macromolecules* **1981**, *14* (1), 212–215.
(13) Yeh, F.; Hsiao, B. S.; Sauer, B. B.; Michel, S.; Siesler, H. W. In-situ studies of structure development during deformation of a segmented poly(urethane-urea) elastomer. *Macromolecules* **2003**, *36* (6), 1940–1954.
(14) Yilgor, I.; Yilgor, E. Structure-morphology-property behavior of segmented thermoplastic polyurethanes and polyureas prepared without chain extenders. *Polym. Rev.* **2007**, *47* (4), 487–510.
(15) Murthy, N. S.; Grubb, D. T.; Zero, K. Structural implications of the elliptical form of small-angle reflections in oriented semicrystalline polymers. *Macromolecules* **2000**, *33* (3), 1012–1021.
(16) Wang, W.; Murthy, N. S.; Grubb, D. T. "Butterfly" small-angle X-ray scattering patterns in semicrystalline polymers are double-elliptical. *Polymer* **2007**, *48* (12), 3393–3399.
(17) Koerner, H.; Kelley, J. J.; Vaia, R. A. Transient microstructure of low hard segment thermoplastic polyurethane under uniaxial deformation. *Macromolecules* **2008**, *41* (13), 4709–4716.
(18) Pathak, J. A.; Twigg, J. N.; Nugent, K. E.; Ho, D. L.; Lin, E. K.; Mott, P. H.; Robertson, C. G.; Vukmir, M. K.; Epps, T. H.; Roland, C. M. Structure Evolution in a Polyurea Segmented Block Copolymer Because of Mechanical Deformation. *Macromolecules* **2008**, *41* (20), 7543–7548.
(19) Sonnenschein, M. F.; Prange, R.; Schrock, A. K. Mechanism for compression set of TDI polyurethane foams. *Polymer* **2007**, *48* (2), 616–623.
(20) Korley, L. T. J.; Pate, B. D.; Thomas, E. L.; Hammond, P. T. Effect of the degree of soft and hard segment ordering on the morphology and mechanical behavior of semicrystalline segmented polyurethanes. *Polymer* **2006**, *47* (9), 3073–3082.
(21) Sonnenschein, M. F.; Lysenko, Z.; Brune, D. A.; Wendt, B. L.; Schrock, A. K. Enhancing polyurethane properties via soft segment crystallization. *Polymer* **2005**, *46* (23), 10158–10166.
(22) Rodriguez, F.; Cohen, C. *Principles of Polymer Systems*, 5th ed.; Taylor and Francis Publishing: New York, 2003; p 760.
(23) Yilgör, E.; Burgaz, E.; Yurtsever, E.; Yilgör, I. Comparison of hydrogen bonding in polydimethylsiloxane and polyether based urethane and urea copolymers. *Polymer* **2000**, *41* (3), 849–857.
(24) Abouzahr, S.; Wilkes, G. L.; Ophir, Z. Structure Property Behavior of Segmented Polyether Mdi Butanediol Based Urethanes - Effect of Composition Ratio. *Polymer* **1982**, *23* (7), 1077–1086.
(25) Rangarajan, P.; Register, R. A.; Adamson, D. H.; Fetters, L. J.; Bras, W.; Naylor, S.; Ryan, A. J. Dynamics Of Structure Formation In Crystallizable Block-Copolymers. *Macromolecules* **1995**, *28* (5), 1422–1428.
(26) Veenstra, H.; Hoogvliet, R. M.; Norder, B.; de Boer, A. P. Microphase separation and rheology of a semicrystalline poly(ether-ester) multiblock copolymer. *J. Polym. Sci., Part B: Polym. Phys.* **1998**, *36* (11), 1795–1804.
(27) E. Kontou, G. S. Interrelation between long-term viscoelasticity and viscoplastic responses of semicrystalline polymers. *J. Appl. Polym. Sci.* **2003**, *88* (8), 1942–1950.
(28) McLean, R. S.; Sauer, B. B. Tapping-Mode AFM Studies Using Phase Detection for Resolution of Nanophases in Segmented Polyurethanes and Other Block Copolymers. *Macromolecules* **1997**, *30* (26), 8314–8317.
(29) Aneja, A.; Wilkes, G. L. A systematic series of "model" PTMO based segmented polyurethanes reinvestigated using atomic force microscopy. *Polymer* **2003**, *44* (23), 7221–7228.
(30) Gogolewski, S. Selected Topics in Biomedical Polyurethanes - a Review. *Colloid Polym. Sci.* **1989**, *267* (9), 757–785.
(31) Garrett, J. T.; Lin, J. S.; Runt, J. Influence of preparation conditions on microdomain formation in poly(urethane urea) block copolymers. *Macromolecules* **2002**, *35* (1), 161–168.
(32) Lee, D. K.; Tsai, H. B. Properties of segmented polyurethanes derived from different diisocyanates. *J. Appl. Polym. Sci.* **2000**, *75* (1), 167–174.

(33) Skarja, G. A.; Woodhouse, K. A. Structure-property relationships of degradable polyurethane elastomers containing an amino acid-based chain extender. *J. Appl. Polym. Sci.* **2000**, *75* (12), 1522–1534.
(34) Xu, L. C.; Soman, P.; Runt, J.; Siedlecki, C. A. Characterization of surface microphase structures of poly(urethane urea) biomaterials by nanoscale indentation with AFM. *J. Biomater. Sci., Polym. Ed.* **2007**, *18* (4), 353–368.
(35) Ji, F. L.; Hu, J. L.; Li, T. C.; Wong, Y. W. Morphology and shape memory effect of segmented polyurethanes. Part I: With crystalline reversible phase. *Polymer* **2007**, *48* (17), 5133–5145.
(36) Gerasimo, Vi.; Genin, Y. V.; Tsvankin, D. Y. Small-Angle X-Ray Study of Deformed Bulk Polyethylene. *J. Polym. Sci., Part B: Polym. Phys.* **1974**, *12* (10), 2035–2046.
(37) Zhu, L.; Cheng, S. Z. D.; Calhoun, B. H.; Ge, Q.; Quirk, R. P.; Thomas, E. L.; Hsiao, B. S.; Yeh, F. J.; Lotz, B. Crystallization temperature-dependent crystal orientations within nanoscale confined lamellae of a self-assembled crystalline-amorphous diblock copolymer. *J. Am. Chem. Soc.* **2000**, *122* (25), 5957–5967.

MA8022052